Bull Volcanol
DOI 10.1007/s00445-006-0106-1

RESEARCH ARTICLE

Ground deformation modeling of flank dynamics prior to the 2002 eruption of Mt. Etna

Alessandro Bonforte · Salvatore Gambino · Francesco Guglielmino · Francesco Obrizzo · Mimmo Palano · Giuseppe Puglisi

Received: 15 December 2005 / Accepted: 4 October 2006

Abstract On 22 September 2002, 1 month before the beginning of the flank eruption on the NE Rift, an M-3.7 earthquake struck the northeastern part of Mt. Etna, on the westernmost part of the Pernicana fault. In order to investigate the ground deformation pattern associated with this event, a multi-disciplinary approach is presented here. Just after the earthquake, specific GPS surveys were carried out on two small sub-networks, aimed at monitoring the eastern part of the Pernicana fault, and some baselines belonging to the northeastern EDM monitoring network of Mt. Etna were measured. The leveling route on the northeastern flank of the volcano was also surveyed. Furthermore, an investigation using SAR interferometry was performed and also the continuous tilt data recorded at a high precision sensor close to the epicenter were analyzed to constrain the coseismic deformation. The results of the geodetic surveys show a ground deformation pattern that affects the entire northeastern flank of the volcano, clearly shaped by the Pernicana fault, but too strong and wide to be related only to an M-3.7 earthquake. Leveling and InSAR data highlight a local strong subsidence, up to 7 cm, close to the Pernicana fault. Significant displacements, up to 2 cm, were also detected on the upper part of the NE Rift and in the summit craters area, while the displacements decrease at lower altitude, suggesting that the dislocation did not continue further eastward. Three-dimensional GPS data inversions have been attempted in order to model the ground deformation source and its relationship with the volcano plumbing system. The model has also been constrained by vertical displacements measured by the leveling survey and by the deformation map obtained by SAR interferometry.

Keywords Ground deformation · Modeling · Flank dynamics · Volcano-tectonics · Pernicana fault · Mt. Etna volcano

Editorial responsibility M. Ripepe

A. Bonforte (✉) · S. Gambino · F. Guglielmino · M. Palano · G. Puglisi
Istituto Nazionale di Geofisica e Vulcanologia,
Sezione di Catania, Pizza Roma 2,
95123 Catania, Italy
e-mail: bonforte@ct.ingv.it

F. Obrizzo
Istituto Nazionale di Geofisica e Vulcanologia,
Oss. Vesuviano, v. Diocleziano 328,
80124 Napoli, Italy

Introduction

The Pernicana fault system is very well known in recent literature on Mt. Etna (Borgia et al. 1992; Lo Giudice and Rasà 1992; Azzaro 1997; Azzaro et al. 2001; Obrizzo et al. 2001). It is described as one of the most active structures in the geodynamic framework of the volcano, and models proposing flank collapse (Borgia et al. 1992; Lo Giudice and Rasà 1992) agree in identifying it as the northern margin of the volcano's sliding flank.

Morphological evidence of the fault can be followed for about 11 km, with an approximate E–W strike (Fig. 1). From west to east, it intersects the NE Rift (1,900 m asl), crossing the Piano Provenzana and Piano Pernicana areas, and reaches the Rocca Campana area (900 m asl), where the fault branches out southeastwards into a splay fault.

The observed direction of displacement varies along the fault trace. At its upslope western end, it is almost pure southward downthrown dip-slip, producing a prominent south-facing scarp up to 80 m high; in the middle part, the slip is left-oblique producing a south-facing scarp about

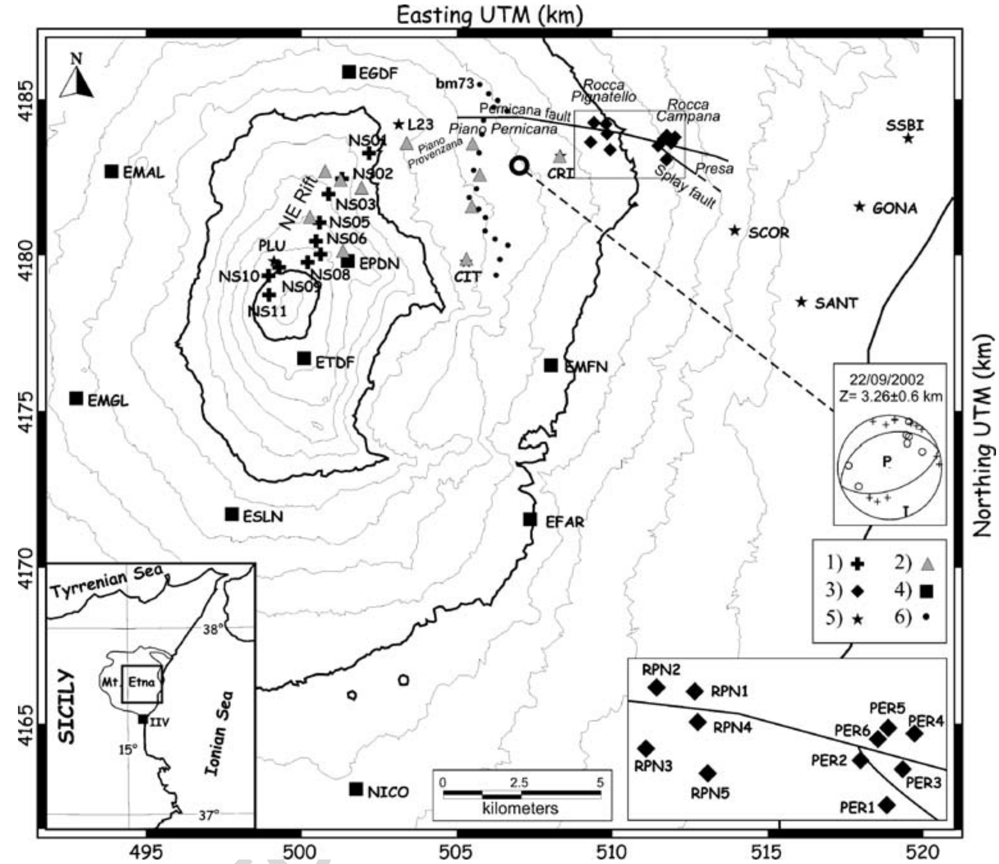

Fig. 1 Mount Etna geodetic networks and main geological features of the northeastern flank of the volcano. Coordinates are in UTM projection, zone 33N. (1) GPS stations belonging to the NS kinematic profile, (2) EDM stations, (3) GPS stations belonging to the Rocca Campana and Rocca Pignatello networks (enlarged in the *box in lower right corner*), (4) GPS permanent stations, (5) GPS stations belonging to the Mt. Etna network periodically surveyed, (6) leveling benchmarks. Location of IIV GPS reference station is also shown. The *open circle* shows the location of the magnitude 3.7 earthquake of 22 September 2002

40 m high; at the east end, up to the village of Presa (see Fig. 1), the displacement is almost pure left-lateral strike-slip, the morphological evidence disappears, and the fault can be detected only by creep-induced damage to man-made features along the dislocation lines.

The western and central segments are seismogenic, with frequent shallow earthquakes, which can reach magnitudes up to 4.2, and cause surface faulting and severe damage to man-made features. The eastern segment of the fault is characterized by aseismic fault movements with evidence of activity revealed by continuous left-lateral displacements having a creep-rate of about 2 cm/year based on historic and geodetic estimations (Azzaro et al. 1998, 2001).

The most recent earthquakes producing large surface fractures were recorded on 25 December 1985 and 29 October 1986, respectively with M 4.0 and M 4.1. Until today, although no further large earthquakes have occurred, a widespread seismicity has characterized the central and western segments of the fault, confirming that the structure is highly active.

On 22 September 2002, an M-3.7 earthquake, whose instrumental epicenter was located a few km south of the westernmost part of the Pernicana fault, struck the northeastern part of the volcano (Fig. 1). This event produced coseismic surface fractures and damage to man-made features in the Piano Pernicana area. In order to measure the ground deformations associated with this event, existing GPS and EDM networks were re-occupied on the northeastern part of the volcano, and the leveling route on the northeastern flank of the volcano was surveyed.

Data

EDM network and surveys

An electronic distance measurements (EDM) network, situated on the northeastern flank of Mt. Etna (Fig. 1), is one of the first geodetic networks installed on the volcano for ground deformation studies at the end of the 1970s. It consists of 15 benchmarks, extending from the summit area down to an altitude of about 1,000 m and is surveyed at least yearly in summer time (Falzone et al. 1988; Nunnari and Puglisi 1997). The distances between the benchmarks of the network range from 1–5 km; the measurements are carried out using a geodimeter AGA 6000 giving a measurement accuracy of 5 mm+1 ppm. Horizontal and vertical angles are also periodically measured by using a Wild DKM3 theodolite.

After the 22 September 2002 earthquake, in the first days of October, several baselines of this network were measured. The selected baselines cross the westernmost end of the Pernicana fault, where this structure joints the rift zone. A few baselines crossing the fault could not be surveyed for meteorological and logistic reasons.

Leveling route and surveys

The leveling route on Mt Etna was installed in September 1980 to monitor the volcano's flanks where eruptive fractures have a high probability of opening. The route is 150 km long, distributed along the mountain roads on the southern, western, and northeastern flanks of the volcano and consists of 200 benchmarks. The benchmarks are generally consolidated either directly into solid lava outcrops or into concrete foundations. The measurements were performed with Wild NA2 levels equipped with optical micrometers and invar rods. We utilized the double-run precise leveling method and the mean error was less than 1.0 mm/km.

Part of the leveling route crosses the Pernicana fault perpendicularly at an altitude of about 1,400 m asl. This segment of the network is 11 km long and consists of 18 benchmarks (Fig. 1). The reference benchmark used to calculate the height variations is the bm73 (see Fig. 1), which lies on the northern side of the fault at a distance of about 1 km from it. The first measurements on this network were carried out in September 1980, and 34 surveys were made up to October 2002. The analysis performed on the height variations resulting by comparing the two surveys encompassing the earthquake (from September 2001 to October 2002) indicates a strong subsidence of the southern part of the fault (foot-wall) with respect to the northern one (Obrizzo et al. 2001, 2004).

GPS networks and surveys

Two geodetic networks based on global positioning system (GPS) techniques, lie across the eastern segment of the Pernicana fault (Fig. 1). The first one, located in the "Rocca Campana" area, was installed in April 1997 and consists of six self-centering benchmarks. More than 20 surveys were made up to September 2002, every 3–4 months, giving considerable detail of the motion of the fault over time. The second one, located a few kilometers westward, in the "Rocca Pignatello" area, was measured for the first time in July 2002; it consists of five self-centering benchmarks that upgrade a pre-existing EDM network (Azzaro et al. 2001). The two networks are relatively small, each one covering an area of about 1 km^2. The aim of these networks is to quantify the structural framework and displacements along the aseismic-creep sector of the Pernicana fault to better constrain its dynamic behavior (Azzaro et al. 2001).

After the 22 September 2002 earthquake, a 4-day-long GPS survey was carried out on the northeastern part of the volcano. The measurements were carried out on both networks (Rocca Campana and Rocca Pignatello), together with some benchmarks belonging to the northeastern part of the inner GPS network of Mt. Etna (Puglisi et al. 1998; Bonforte and Puglisi 2003), the northernmost stations of the "Ionica" network and the northern half of the N–S kinematic profile (Table 1).Instruments used were Trimble receivers (models 4000 SSI, 4000 SSE, and 4700) and Trimble antennas (Choke Ring and Compact with ground plane models).

GPS data collected during the surveys were processed together with those coming from the Mt. Etna permanent GPS network (Fig. 1). Trimble Geomatics Office package v. 1.5, manufactured by Trimble, was adopted to process the data, using precise ephemerides computed by the National Geodetic Survey of the National Oceanic and Atmospheric Administration (NOAA's NGS) and distributed through Navigation Information Service (NIS) as usually adopted for GPS surveys on Mt. Etna (Puglisi et al. 1998; Bonforte and Puglisi 2003). The GPS data processing was performed by computing each baseline independently.

The baseline solutions were then adjusted to obtain station coordinates with their associated errors. The adjustment was performed using all baseline solutions, treating the IIV station (belonging to the GPS reference network of Mt. Etna) as fixed, to detect displacements affecting the measured stations relative to a stable reference (Puglisi et al. 2004).

The comparison between the results of the GPS survey carried out in September 2002 and those of July 2002 shows a ground deformation pattern that affects the whole northeastern flank of the volcano (Fig. 2). The pattern is clearly shaped by the Pernicana fault; displacements of about 2–3 cm affect all stations lying on the southern side of the fault at the Rocca Pignatello and Rocca Campana networks. Furthermore, the different magnitude of bench-

Table 1 Stations surveyed during the GPS survey carried out after the earthquake

Date	Stations			
25 September 2002	SCOR	GONA	SSBI	SANT
	L23	CRI	RPN1	RPN2
	RPN3	RPN4	RPN5	
26 September 2002	L23	CRI	RPN1	RPN2
	RPN3	RPN4	RPN5	
27 September 2002	CRI	RPN1	RPN2	RPN4
30 September 2002	NS01	NS02	NS03	NS05
	NS06	NS07	NS08	NS09
	NS10	NS11	L23	PLU

Fig. 2 Displacements at the GPS station between 1 July and 25 September 2002

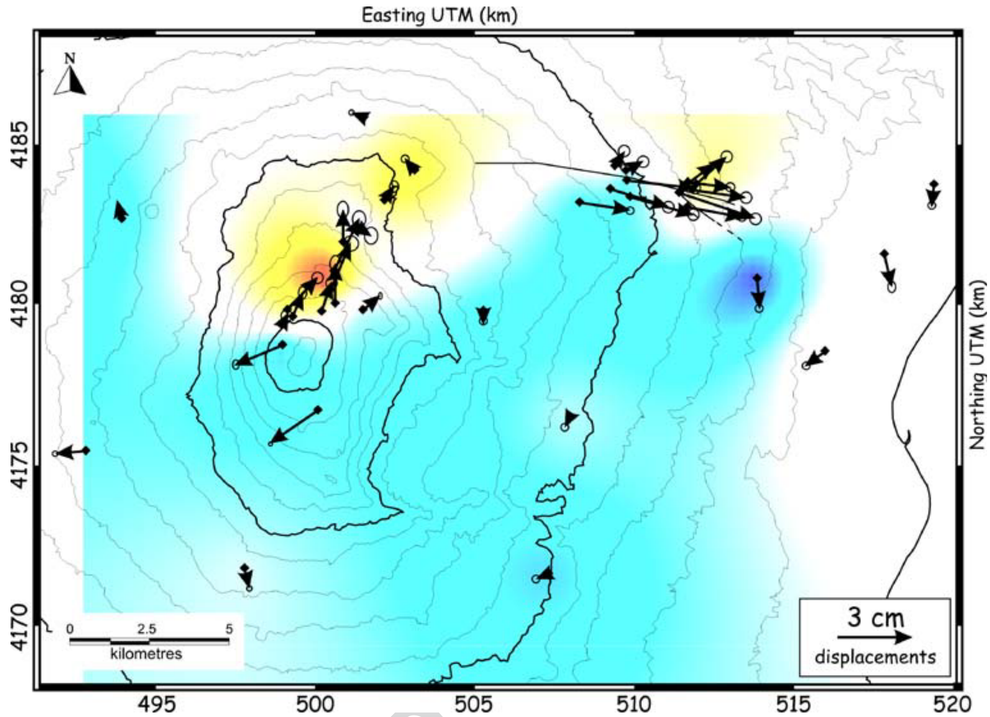

mark PER3 (Rocca Campana network, see inset in Fig. 1) with respect to those of benchmarks PER1 and PER2, indicates the partition effect induced by the splay fault, which accommodates the displacement of the Pernicana fault. Unexpected significant displacements, up to 2 cm, were also detected in the upper part of the NE Rift and the summit area.

DInSAR data

The DInSAR data processing was performed using the image processing tools developed by Atlantis (EarthView InSar v. 2.0). We used SAR data from European Space Agency's (ESA) ERS2 satellite, equipped with a C band SAR with a wavelength of 5.6 cm. The procedure used for the generation of interferometric products relevant to the selected image pairs is called "two pass interferometry" (Massonet and Feigl 1998). With this method, two SAR scenes are used to generate a real-phase interferogram that is correlated with topography and changes in topography. To analyze the topographic changes, the topography-dependant part of the phase needs to be eliminated; this requires the use of a DEM. The elevation values provided by the DEM need to be converted into synthetic phase-values. In the next step, the phase-values of the real and synthetic interferograms have to be subtracted from each other. In this way, residual phase-values are obtained, resulting in a differential interferogram, which is correlated to the changes in topography (i.e., deformation) and possibly tropospheric noise.

The advantage of this approach is that it removes many unwanted fringes, leaving only those related to the signal of interest and/or errors in the DEM. The photogrammetric DEM used as a source for the topographic information has a measured accuracy of the order of 10 m. To co-register the two images and calculate the interferometric geometry, we used the precise orbits of the ERS2 satellite, produced at the Delft Institute for Earth Oriented Space Research (DEOSR). The interferogram is projected into an orthogonal geographic coordinate system, so that users need not work with distorted radar geometry.

The two ascending ERS2 passes (31 July 2002 and 9 October 2002) used to generate the interferogram have a perpendicular baseline (i.e., the distance between the orbits) of only 2 m. This produces a "height ambiguity" of 4,400 m; this means that the interferogram is sensitive to topographic errors equal to or larger than 4.4 km! With a 10-m DEM error, the phase error is less than 0.1 mm, so the actual interferogram is insensitive to topographic errors. Finally, the short temporal (3 months) and spatial baselines produced good coherence even on vegetated areas such as the northeastern flank of the volcano. The tropospheric noise could not be removed but the resulting effect does not exceed half a fringe; furthermore, DInSAR data are here compared with GPS and leveling data, helping us to distinguish between atmospheric artifacts and ground motion.

The differential interferogram is shown in Fig. 3a. In this case, each fringe corresponds to a displacement of 2.8 cm of the ground surface along the line of sight (LOS) of the

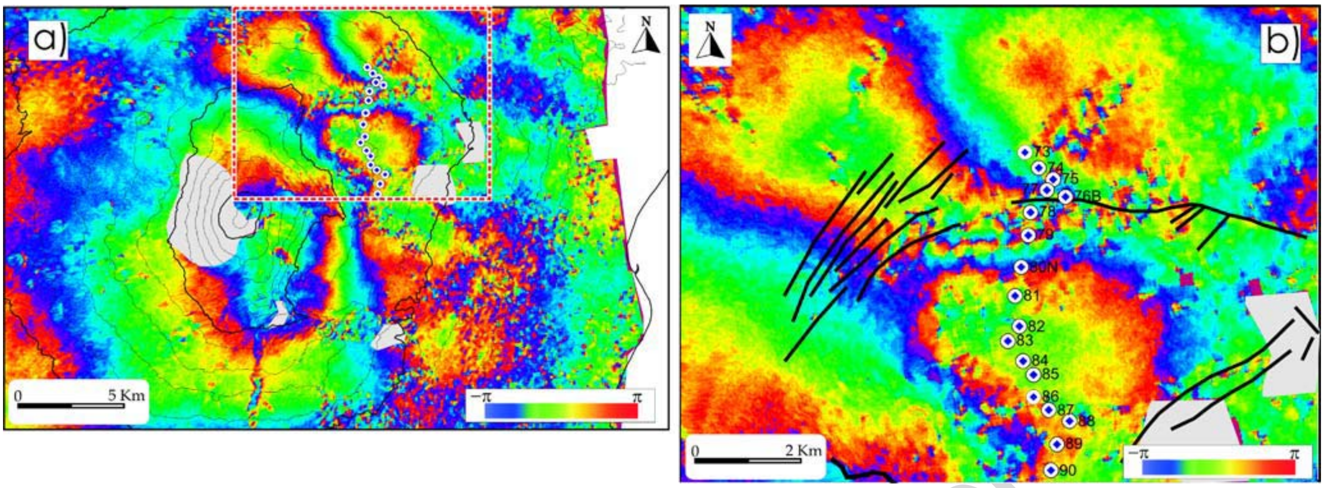

Fig. 3 Differential interferogram for ascending scene pair 31 July 2002 to 09 October 2002: **a** phase interferogram; **b** enlargement of the Pernicana area, *circles* indicate the leveling stations. The scale indicates the phase variation along the LOS (negative values correspond to the approaching of the surface to the sensor)

radar sensor; this means that on the interferogram we can read how the Earth surface moves away or approaches the sensor. Since the radar view angle is 23° off nadir, SAR interferometry is more sensitive to vertical movements.

Tilt data

The Mt. Etna permanent tilt network (Fig. 4a) comprises nine bi-axial instruments installed in shallow boreholes at about 3 m depth, and one long baseline instrument (Bonaccorso et al. 2004).The borehole instruments use a high precision electrolytic bubble sensor to measure the angular movement and are equipped with AGI model 510 tiltmeters with a precision of 0.01 μrad, or model 722, with a precision of 0.1 μrad. The long-base tilt instrument is composed of a mercury filled tube, positioned inside two 80-m-long artificial underground orthogonal tunnels at the Volcanological Observatory of Pizzi Deneri, located 2,850 m asl on the northeastern flank of Mount Etna volcano (3340 m asl), 2 km away from the summit craters.

The fluid-filled tube is connected to three beakers at the two extremities and in the central part of the tunnels; optical laser sensors, fixed at the top of each beaker, are used to measure mercury level changes. Resolution of the instrument is about 0.01–0.05 μrad and data sampling is 144 data/day (48 data/day for bore-hole stations).

Shallow borehole tiltmeters are affected by noise related to local instabilities or daily and seasonal temperature changes that may mask small changes or slow deformation with a short to medium period (from weeks to months) linked to geophysical processes. Otherwise, long-base devices can record very stable high-precision signals characterized by very low noise. The Mt. Etna long baseline instrument has been able, in recent years, to also detect small variations related to seismic, eruptive, and explosive events (Bonaccorso et al. 2004).

For the period analyzed here from July to September 2002, we considered only signals recorded at the PDN long base tiltmeter (Fig. 4) that showed a clear continuous drop in the radial component (Fig. 4b). In the signals recorded at the other tilt stations, due also to the higher noise level, no significant variation is visible.

Data analysis and inversions of ground deformation data

The only significant data relevant to the earthquake itself is the tilt at PDN station (Fig. 4a, b). Although only one datum is not sufficient to deduce any source parameter, the PDN signal shows an evident coseismic variation that can be usefully exploited to check the agreement with the source suggested by seismic data. The PDN tilt station showed a coseismic tilt of about 1 μrad (Fig. 4c) concomitant to the strong local earthquakes (Ml=3.7) recorded on 22 September at 16:01 local time by the INGV local permanent seismic network (Gambino et al. 2004). The focal solution obtained using the FPFIT algorithm (Reasenberg and Oppenheimer 1985) shows a normal mechanism along a N70°E plane with a SSE 55° dip (Fig. 4d).

An estimate of the seismic moment release and source dimension associated with the event was obtained using the spectral analysis (omega-zero level and and corner frequency) of the seismic signal recorded at EMF seismic station (Fig. 4a, e). Source parameters have been estimated after the application of instrumental, attenuation, and geometrical spreading corrections on P-wave displacement spectra

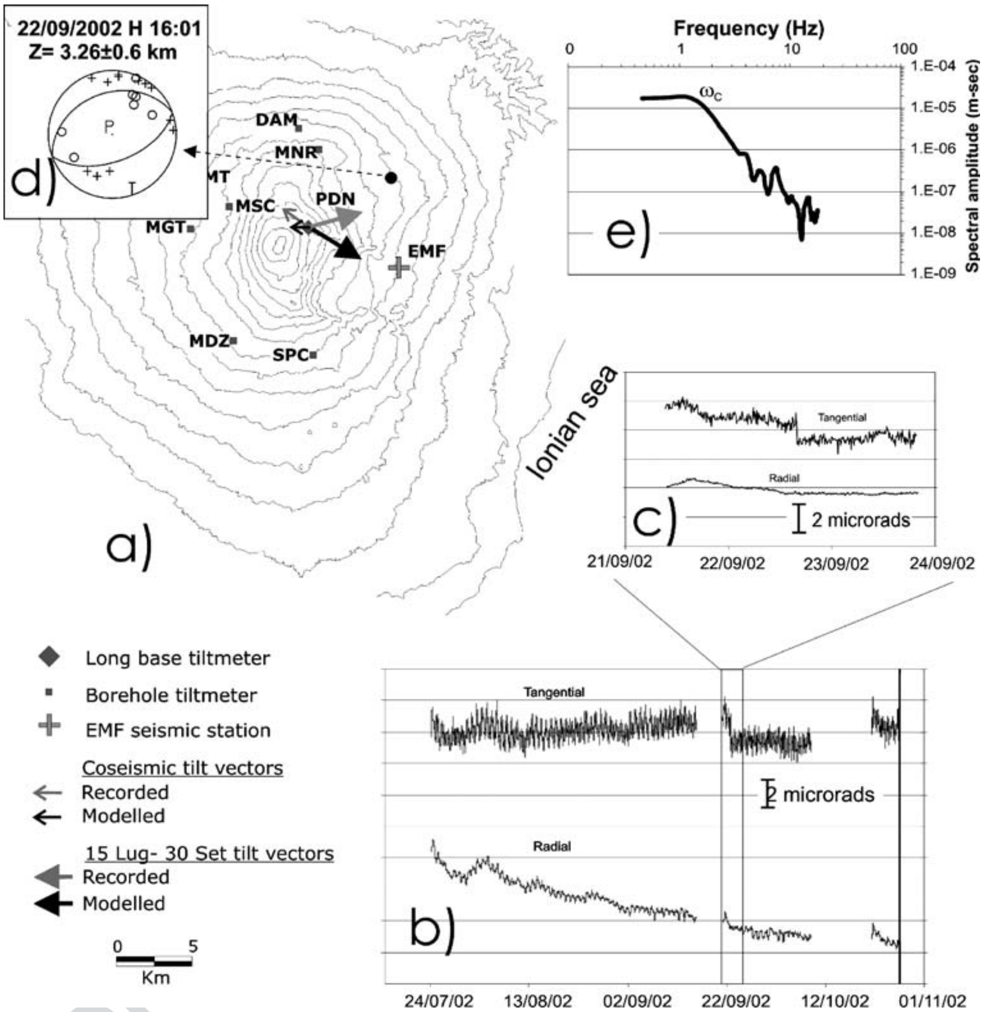

Fig. 4 **a** Mount Etna permanent tilt network with recorded and expected tilt vectors at PDN station. **b** Tilt signals recorded at PDN station; with tilt radial to the summit (positive means summit up) and tangential tilt (positive means uplift anticlockwise). **c** Coseismic tilt variation at PDN station. **d** Focal solution of the 22 September 2002 earthquake. **e** P-wave displacement spectrum

(Fig. 4e). The seismic moment obtained by omega-zero level (Brune 1970) is 3.6×10^{21} dyne × cm, while a fault radius of 0.8 km has been estimated using the corner frequency (Brune 1970).

The average slip has been obtained by the general relation (Aki 1966):

$$Mo = \mu * S * \bar{u}$$

As medium rigidity is not well known, we considered a value ranging from 10^{11} dyne/cm^2 (Bonaccorso and Patanè 2001) to 2×10^{11} dyne/cm^2 obtaining an average slip $\bar{u}$ of about 1–2 cm.

Taking these results (fault area and average slip) into account, we computed ca. 0.3–0.5 μrad of expected tilt change (at PDN station) (Fig. 4a) for a tabular dislocation model (Okada 1985) striking N70°E, dip 55°, located at the earthquake hypocenter.

The recorded and expected (from the model) tilt vectors are comparable in magnitude and show slightly different directions (Fig. 4a). Conversely, the slip observed along the fault (R. Pignatello and R. Campana areas) from July to September is more than that expected from an M-3.7 earthquake. The average slip measured by GPS measurements is of the order of 2–3 cm over a period of about 2 months, while the surface movements that the earthquake should produce from the above model, are of the order of 1 mm. The resulting measured slip rate is of the order of 10 cm/year. Compared with the mean rate measured after the 2001 eruption, this value does not indicate a significant short-term acceleration. Furthermore, even in the years pre-2001, acceleration was sometimes observed, not necessarily associated to volcanic or seismic events (Azzaro et al. 2001; Fig. 5).

The comparison between the EDM measurements carried out in October 2002 and those carried out on the entire network in June 2002 (Fig. 6) shows significant deformation only on the lines crossing the western end of the Pernicana fault. The only variations exceeding the experimental error of 5 mm+1 ppm are extensions, measured on the slope distances connecting Mt. Nero, Bocche 1809, C. Linguaglossa and Pizzi Deneri benchmarks, on the northwestern side, with R. Puchoz, Due

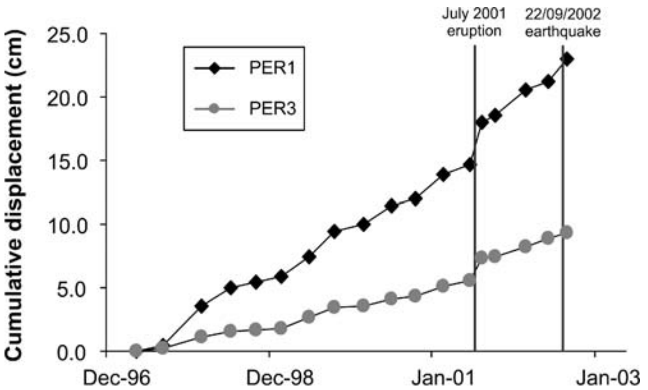

Fig. 5 Slip rate measured at "Rocca Campana" GPS network since 1997. The displacements are referred to PER5 benchmark (see Fig. 1)

Monti, Lave 1865, R. Citelli and M. Crisimo benchmarks, on the southeastern side of the fault. These extensions range between 1.3 and 3.1 cm.

The comparison of the two leveling surveys (Fig. 7) shows an abrupt vertical displacement of the southern side of the Pernicana fault, with a local maximum subsidence of −65 mm very close to the fault plane, rapidly decreasing to zero about 2 km to the south. The southernmost part of the route shows a slight uplift of less than 10 mm. As with the tilt data, the measured ground deformation seems larger than expected from the model of the M-3.7 earthquake, even if we consider that the time since the previous leveling survey is longer; from September 2001 to October 2002.

A preliminary analysis of the interferogram (Fig. 3) shows relative stability in the imaged area, especially taking into account the uncertainty of half a fringe due to instrumental and atmospheric effects, apart from a SE–NW elongated area in the upper part of the Pernicana fault, between the Piano Provenzana and the Piano Pernicana areas, and shown in detail in the inset, Fig. 3b. Here, a gradient of three fringes between benchmarks 76B and 80N induces a maximum dislocation of about +8 cm along the line of sight of the SAR sensor, on the southern side of the fault. DInSAR ground deformation data at the pixels corresponding to the leveling benchmarks are compared to leveling values in Fig. 7. The measurements are in good agreement, showing relative stability of the area, apart from a very local subsidence just south of the Pernicana fault. The stronger deformation measured by DInSAR at benchmarks 78, 79 and 80N is perhaps due to the horizontal component of motion. In the eastern part of the interferogram, a progressive increase of the ground-satellite distance of the order of 1.5 fringes, is visible. This type of fringe pattern is known from previous ERS observations of Mt. Etna and has been interpreted as a local effect of the Pernicana fault (Lundgren et al. 2003).

All the above data depict ground movement in relatively small areas and are most probably not produced by the M-3.7 earthquake alone, because the displacement is too large. Together with the significant ground deformation measured by GPS network, this suggests that the origin of this complex ground deformation pattern measured during the months encompassing the earthquake, is not just related to the seismic event. To investigate the origin of this pattern, the GPS data shown in Fig. 2 were inverted, because they are the only data suitable for an analytic inversion of sufficient detail to deduce source locations with confidence.

Fig. 6 Baseline variations measured by EDM between June and October 2002

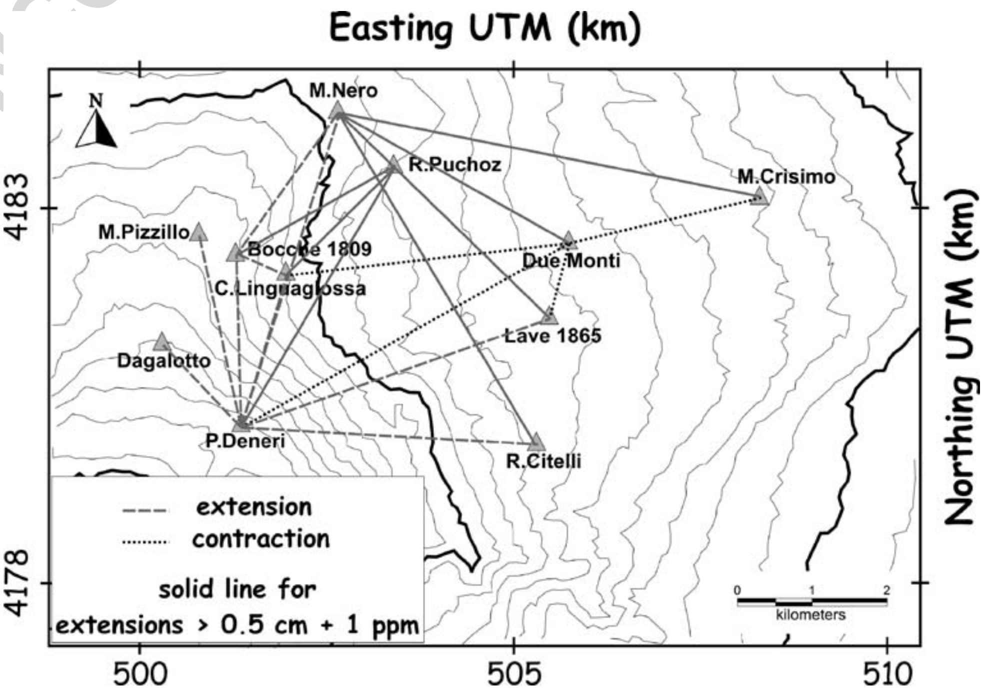

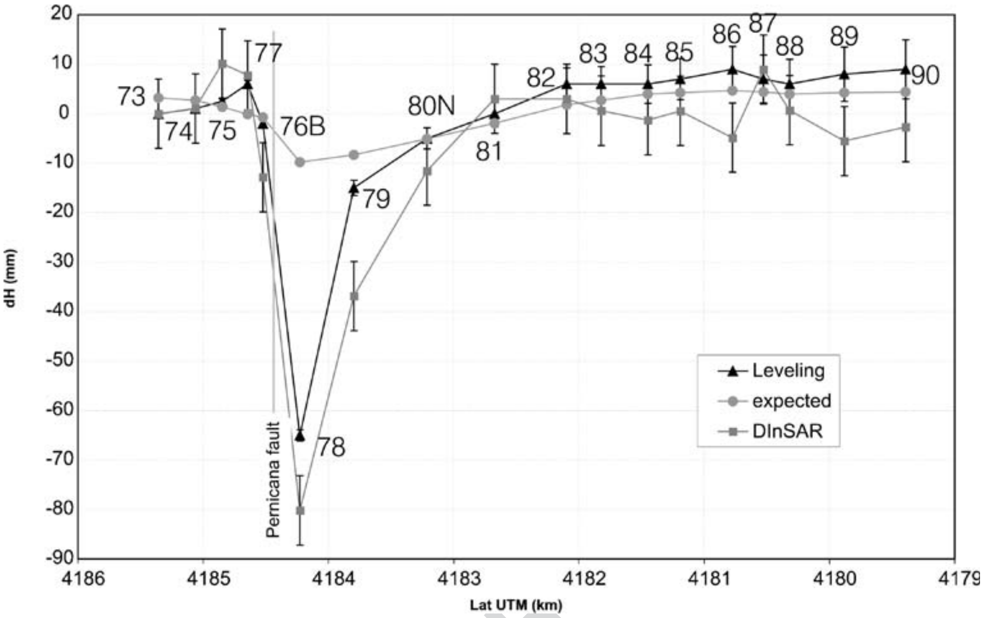

Fig. 7 Measured and expected (from the model) vertical displacements along the leveling route. The LOS displacements measured by DInSAR are also reported

GPS provides three-dimensional displacement measurements across the entire deformed area within a relatively short-time interval (3 months) encompassing the seismic event. The other ground deformation data (i.e., leveling, InSAR, EDM, and tilt) is useful in refining the model obtained from GPS data.

The Okada (1985) dislocation model and a least squares algorithm (LQA) were used to perform the data inversions, using a procedure that has been successfully applied to Mt. Etna GPS data (Puglisi et al. 2004 and references herein). The use of the Okada model requires the estimation of 10 dislocation parameters: its three-dimensional position, dimensions, orientation of both azimuth and dip, displacement of strike slip and dip slip and opening, and width. The use of LQA needs an appropriate set of starting values for each source parameter, as close as possible to the true value. To this end, available broad geological information is taken into account.

Visual inspection of the GPS displacement vectors (Fig. 2) suggests that besides the Pernicana and splay faults, there could be at least three other sources in the higher part of the volcano. Firstly, the NE Rift, secondly the structural link between the Pernicana and the NE Rift in the area of Piano Provenzana, and thirdly beneath the summit craters. The latter probably tensile, judging from the displacement vectors measured at the uppermost stations of the N-S kinematic profile and the TDF permanent station. The inversion was therefore performed using five dislocation sources, excluding the fault producing the earthquake, because the very small movements expected from this source are within the errors of the GPS surveys. The first two sources, in the central eastern part of the Pernicana fault, were located in position, azimuth, and length, using field evidence. The other three sources: the NE Rift, the Provenzana, and the summit craters dislocations were positioned as shallow vertical planes bordering the sliding sector of the NE Rift and beneath the summit craters. The azimuth of the summit craters dislocation was oriented approximately perpendicular to the displacement vectors, and the motion was fixed as pure tensile. The Provenzana fault trend, clearly visible in the field was then added to fit the very local deformation measured by EDM, InSAR, and leveling.

In Fig. 8, the location of the sources and the relevant expected horizontal displacement vectors are shown as are the comparisons with EDM data in Table 2. The final parameters of the model are given in Table 3.The expected vertical displacements fit the leveling measurements well, except for the very local deformation observed close to the Pernicana fault (Fig. 7), where the leveling line shows a greater subsidence than the model. The good agreement between leveling and InSAR confirms that an intense local deformation episode occurred close to the Pernicana fault, perturbing the ground deformation pattern expected from the theoretical model. Just 1 km south of the fault, the misfit between the expected and measured displacements is within the errors. These considerations represent a strong validation of both the model and dataset.

Discussions

GPS, EDM, leveling, and DInSAR data analyzed in this paper depict a very complex ground deformation pattern resulting from the intersection of several individual patterns, each one characterized by different temporal and spatial wavelength and intensity. As far as the earthquake is concerned, it produced a much weaker ground deformation

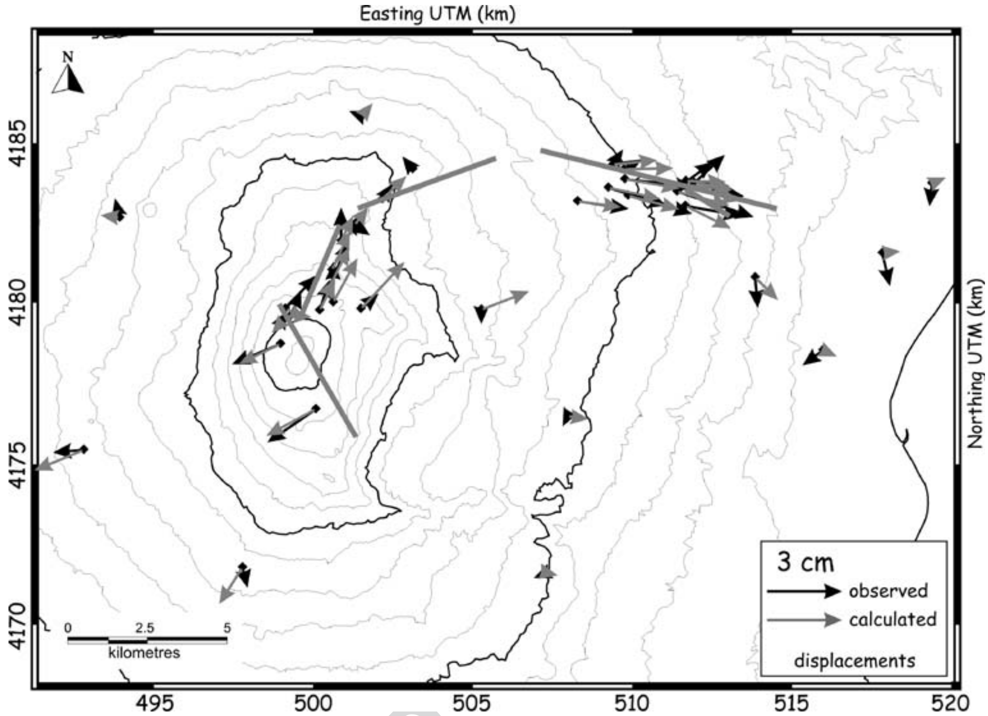

Fig. 8 Expected and measured displacements for the GPS network. The modeled structures are also shown. Coordinates are in UTM projection, zone 33N

t2.1 **Table 2** Observed and calculated length variations at EDM benchmarks

	EDM lines	Measured variations (cm)	Expected variations (cm)
t2.2			
t2.3	C. Linguaglossa–Due Monti	−0.2	−0.1
t2.4	P. Deneri–Due Monti	−0.2	−0.4
t2.5	P. Deneri–R. Citelli	0.7	0.5
t2.6	Lave 1865–Due Monti	−0.4	0.0
t2.7	P. Deneri–Lave 1865	0.9	−0.1
t2.8	M. Pizzillo–P. Deneri	0.3	−1.0
t2.9	Dagalotto–P. Deneri	0.2	−0.1
t2.10	P. Deneri–R. Puchoz	1.3	−0.8
t2.11	Bocche 1809–P. Deneri	0.2	−0.7
t2.12	Bocche 1809–R. Puchoz	2.8	0.0
t2.13	Due Monti–M. Crisimo	−0.9	−0.5
t2.14	C. Linguaglossa–Lave 1865	0.0	0.3
t2.15	C. Linguaglossa–R. Puchoz	2.4	−0.5
t2.16	P. Deneri–C. Linguaglossa	0.7	−0.3
t2.17	Bocche 1809–C. Linguaglossa	0.7	0.2
t2.18	M. Nero–Due Monti	2.5	1.6
t2.19	M. Nero–M. Crisimo	1.6	1.8
t2.20	M. Nero–Lave 1865	2.5	1.8
t2.21	M. Nero–R. Citelli	3.1	1.9
t2.22	Bocche 1809–M. Nero	−0.1	−0.2
t2.23	P. Deneri–M. Nero	−0.3	−0.6

field, giving rise to millimetric movements also close to the epicenter area. The only instrumental data relevant to this pattern is from the very sensitive long-base tilt station, about five km away from the epicenter, which measured a tilt of about 1 μrad.

Conversely, very intense but local deformations were measured by the leveling and InSAR techniques close to the Pernicana fault, in the area between the Piano Pernicana and the Piano Provenzana, probably linked to instability along the fault plane triggered by the earthquake. Several conditions could favor such phenomenon: first of all, the topographic and structural conditions, and/or the properties of the outcropping rocks. This area is located near the junction between the Pernicana fault and the NE Rift zone, which is defined by several southeasterly dipping right-stepping *en échelon* extensional fractures (Tibaldi and Groppelli 2002). The fault displacements measured by Tibaldi and Groppelli (2002) here in recent decades clearly indicate an oblique movement (mainly a normal dip-slip with a significant left-lateral component) along the Pernicana fault. Certainly, these sliding movements are facilitated by the scoria outcropping in this area. The instability seems to be confirmed by the subsidence of the benchmark located just north of the fault (Fig. 7). Since this benchmark lies on the footwall of the fault, it is reasonable to relate its motion to sliding of the unstable fault scarp. Our data and the geological framework summarized above are also consistent with the very large movements observed by Acocella et al. (2003) in this area using strainmeters installed in the wall bordering the road that has clearly been affected by instability. The local uplift measured by

Table 3 Parameters of the modelled sources for the eastern part of the Pernicana fault

	Tensile fault	NE Rift	Provenzana fault	Pernicana fault	Splay fault
Longitude (km)	500.200±0.2	499.900±0.2	503.650±0.04	510.590	512.200
Latitude (km)	4178.100±0.3	4181.300±0.2	4183.890±0.03	4183.930	4183.400
Azimuth	N150°E	N23°E	N70°E	N104°E	N123°E
Depth (km asl)	0.9±0.3	1.1±0.2	1.2	0.9±0.02	0.96±0.02
Length (km)	4.8±0.4	3.2±0.3	4.6±0.4	7.6	1.0
Width (km)	4.7±0.3	1.6±0.2	2.6±0.1	2.3±0.1	1.6±0.1
Dip	77°±2°	60.8°±3°	60°±2°	58°±2°	81.8°±2°
Strike slip (>0 if left-lateral) (cm)	0	1.6±0.3	0.5±0.2	2.9±0.3	2.9±0.5
Dip slip (>0 if normal) (cm)	0	3.4±0.4	4.0±0.5	−0.7±0.5	0.6±0.3
Opening (cm)	17.2±2.3	−2.2±0.8	0.5±0.2	1.2±0.3	1.5±0.3

SAR northwest of the Provenzana area (including the NE Rift; Fig. 3b) is outside the area monitored. This unfortunately prevents any meaningful discussion on the origin of this unexpected feature. A simple analytical model predicts an uplift of the same magnitude as the subsidence measured on the hangingwall (benchmark 78), due to the normal movement of the Pernicana fault. The available data do not confirm either that this interferometric feature is a tropospheric effect or that it is produced by deformation related to local dynamics of the NE Rift. It is remarkable that this area corresponds to the lower part of the eruptive fissure field opened 1 month later.

The GPS data inversion also indicates broader ground deformation pattern. The movements of the five planar structures produce a general eastward motion of the northeastern sector of Mt. Etna. The moving sector is bounded westward by the Provenzana fault–NE Rift system, which behaves mainly as a normal fault, and northward by the left-lateral transcurrent Pernicana fault. Southwestward it is bounded by a tensile structure that could indicate shallow intrusion of a dyke beneath the summit craters (Fig. 8).

The general eastward motion is accompanied by a westward tilt of the sliding block, as shown by the data from the PDN tilt station (Fig. 4), and a lowering of the NE Rift. The rotation of this block is also clear both by the normal behavior of the Provenzana fault–NE Rift system and by the left-lateral behavior of the Pernicana fault (see fault parameters in Table 3). It is also confirmed by EDM measurements on the upper part of this flank of the volcano, which show significant extensions of the lines crossing the NE Rift and the uppermost part of the Pernicana fault. The EDM measurements, generally agree with the GPS excluding those baselines involving the R. Puchoz benchmark, which is very close to the uppermost part of the Pernicana fault. This misfit is probably due to the non-elastic behavior of the medium so close to the fault.

All the above considerations lead us to hypothesize that the earthquake resulted from the movement of the entire northeastern flank of the volcano rather than its cause. Also the tilt station did not measure any evident change in the trend of motion after the earthquake, highlighting how the coseismic ground deformation is much less significant than that occurring before and after the earthquake, as observed by GPS, EDM, leveling, and InSAR techniques. This confirms the hypothesis that the earthquake was not an exceptional event and did not represent a change in the dynamics of the volcano.

Although this study does not deal with the origins of the eastward movement of the eastern flank of Mt. Etna, it is indisputable that this movement exists, as confirmed by several geological and geophysical studies. This motion is supposed to originate from gravity (e.g., the weight of the plutonic intrusion beneath the volcano or the mass of the eastern flank) and/or from the pressure induced by magmatic intrusion into the volcanic edifice. GPS and InSAR data have extended the knowledge of the eastward sliding of the eastern flank, pointing out that it exists together with the southward displacement of southern flanks (Froger et al. 2001; Bonforte 2002; Bonforte and Puglisi 2003; Palano 2003). These slow movements are active even without any evidence of shallow intrusions, so that an independent source with respect to the current volcanic activity is the most probable origin in the long term. Furthermore, these movements require two near-horizontal detachment surfaces modeled at depths of about 2 and 0.5 km (Bonforte 2002; Bonforte and Puglisi 2003). However, Bonforte and Puglisi (2003) didn't exclude the possibility that shallow intrusions might accelerate the motions, producing significant slips along fault surfaces, e.g., as observed during the 2001 eruption (Bonforte et al. 2004) and seismic stress release along the Pernicana fault, e.g., the case of the 1994 earthquake (Puglisi et al. 2001). However, the data discussed here suggest that this is not the case for the September earthquake, because the two local networks at Pernicana do not show any significantly strong acceleration. The slip rate measured for the July–September period is indeed rather higher than the mean slip rate of the fault, but falls within the range of variation observed since 1996 (Fig. 5). Other periods characterized by higher slip rates have been detected (e.g., in 1999), accompanied by no significant seismic events; and in any case, the acceleration accompanying the 22 September 2002, earthquake was not comparable to that produced by the 2001 dyke intrusion that produced almost twice the usual slip rate, even though the eruptive fissures opened on the southern flank of the volcano far from the Pernicana area. These considerations indicate that the earthquake released the energy accumulated along a particular segment of the Pernicana fault (or some other structure linked to it) by widespread and continuous eastward sliding of this flank of the volcano during the summer of 2002.

Regarding the summit tensile structure, it is probably an effect of the eastward and southward motion of the eastern flanks of the volcano because its trend and the tensional component are compatible with the movements of the two near-horizontal detachment surfaces modeled by Bonforte and Puglisi (2003).The movements of these two surfaces produce a depressurization in the upper part of the volcano along a NNW–SSE trend, allowing the subsequent ascent of magma towards the surface. It is noteworthy that the lateral eruption, which started about 1 month after 22 September 2002, was triggered by a fast-evolving dyke located at the southern end of the intrusion modeled here, having similar depth, trend, and dip (Aloisi et al. 2003). In conclusion, we interpret this tensile structure as a dyke formed in the same area as the intrusion that led to the 2001 eruption, confirming that the NNW–SSE trend in the upper southern flank of the volcano is the preferential path for shallow magmatic ascent, even for recent volcanic activity (Puglisi and Bonforte 2004).

Finally, earthquake and intrusion occurring on Mt. Etna in the summer of 2002 seem to originate from the eastward motion of the eastern flank. This motion, together with that of the southern flank, is nearly continuous on Mt. Etna, and GPS data do not show any significant acceleration in the summer of 2002, so that eastward sliding cannot be considered the direct cause of the eruption occurring 1 month after the earthquake, as suggested, for instance, by Acocella et al. (2003). However, this motion certainly broadly facilitated the eruption onset for several reasons. First, the intrusion modeled by GPS data “prepared” the path for the uprising magma along a NNW–SSE trend, in which the dyke feeding the eruption intruded (Aloisi et al. 2003). Furthermore, the extension detected on the Provenzana fault–NE Rift system weakened this flank of the volcano, facilitating the very fast intrusion of the batch of magma coming from the summit conduit, along the NE Rift, feeding the vents of the eruption of 28 October to 3 November 2002. Finally, if the earthquake released the stress accumulated along a locked segment of the Pernicana fault that was resistant to sliding, it allowed the eastward motion to continue.

Conclusions

The 22 September 2002 earthquake spurred three field campaigns and five ground deformation techniques to define the strain pattern associated with this event. The results of these researches throw new light on the dynamics of Mt. Etna just before the onset of the 2002–2003 eruption.

A first remarkable result is that the ground deformation pattern detected by integrating GPS, EDM, leveling, and DinSAR is too big (both in intensity and extension) for an M-3.7 earthquake. The coseismic tilt variation produces significant effects only at the PDN station (a high precision long-base tiltmeter). The expected ground deformation produced by the earthquake source alone, as deduced by seismic data, is too small to be measured by GPS, leveling, EDM surveys and by DInSAR measurements.

To investigate the true origin of this unexpected pattern, GPS displacement vectors from a 2-month period encompassing the seismic event were inverted. The results show a transcurrent fault-system (the Pernicana), a normal fault-system (the Provenzana–Rift system) and an intrusion bounding the eastward moving northeastern sector of Mt. Etna. Whatever the origin of this eastward motion, which is nearly continuous on Mt. Etna, it did not significantly accelerate in the late summer of 2002; even if some local effects, due to the instabilities along the fault plane triggered by the earthquake, emphasizes the coseismic deformation at the surface. We may thus affirm that the earthquake was a result of the continuous motion that had accumulated stress along a locked segment of the fault, rather than the cause of the measured ground deformation pattern.

The complex of structure resulting from these inversions coincide with the principal structures that were active during the early days of the 2002–2003 eruption: the NNW–SSE trending tensile plane that apparently facilitated the injection of the dyke triggering the eruption, the Provenzana–NE Rift system that was intruded in a few hours on 28–29 October, and the Pernicana fault that moved about 0.6 m from 27–28 October. In that context, the dynamics of Mt. Etna in the summer of 2002 resulted in optimal conditions for the onset of the 2002–2003 eruption.

Acknowledgements The Authors are grateful to the two anonymous reviewers for their useful criticism and suggestions that improved our work. This work has been carried out in the framework of the INGV-DPC “Etna” project.

References

Acocella V, Behncke B, Neri M, D'Amico S (2003) Link between major flank slip and 2002–2003 eruption at Etna (Italy). Geophys Res Lett 30:2286. DOI 10.1029/2003GLO18642

Aki K (1966) Generation and propagation of G waves from Niigata earthquake of June 16, 1964, II. Estimation of earthquake moment, released energy, and stress-strain drop from the G wave spectrum. Bull Earthq Res Inst Univ Tokyo 44:73–88

Aloisi M, Bonaccorso A, Gambino S, Mattia M, Puglisi G (2003) Etna 2002 eruption imaged from continuous tilt and GPS data. Geophys Res Lett 30(23):2214. DOI 10.1029/2003GL018896

Azzaro R (1997) Seismicity and active tectonics along the Pernicana fault, Mt. Etna (Italy). Acta Vulcanol 9:7–14

Azzaro R, Ferrelli L, Michetti AM, Serva L, Vittori E (1998) Environmental hazard of capable faults: the case of the Pernicana Fault (Mt. Etna, Sicily). Nat Hazards 17:147–162

Azzaro R, Mattia M, Puglisi G (2001) Dynamics of fault creep and kinematics of the eastern segment of the Pernicana fault (Mt. Etna, Sicily) derived from geodetic observations and their tectonic significance. Tectonophys 333:401–415

Bonaccorso A, Patanè D (2001) Shear response to an intrusive episode at Mt. Etna volcano (January 1998) inferred through seismic and tilt data. Tectonophys 334:61–75

Bonaccorso A, Campisi O, Falzone G, Gambino S (2004) Continuous tilt monitoring: a lesson from 20 years experience at Mt. Etna. In: Bonaccorso A, Calvari S, Coltelli M, Del Negro C, Falsaperla S (eds) Mt. Etna: volcano laboratory. Am Geophys Union Geophys Monogr 143:307–320

Bonforte A (2002) Study of the northeastern sector of the Hyblean plateau and of the eastern flank of Mt. Etna by GPS spatial techniques. PhD Thesis, Università degli Studi di Catania, Catania, Italy

Bonforte A, Puglisi G (2003) Magma uprising and flank dynamics on Mt. Etna volcano, studied by GPS data (1994–1995). J Geophys Res 108:2153–2162

Bonforte A, Guglielmino F, Palano M, Puglisi G (2004) A syn-eruptive ground deformation episode measured by GPS, during the 2001 eruption on the upper southern flank of Mt. Etna. Bull Volcanol 66:336–341

Borgia A, Ferrari L, Pasquarè G (1992) Importance of gravitational spreading in the tectonic and volcanic evolution of Mount Etna. Nature 357:231–235

Brune JN (1970) Tectonic stress and the spectra of seismic shear waves from earthquakes. J Geophys Res 75:4997–5009

Falzone G, Puglisi B, Puglisi G, Velardita R, Villari L (1988) Componente orizzontale delle deformazioni lente del suolo nell'area del vulcano Etna. Boll GNV 4:311–348

Froger JL, Merle O, Briole P (2001) Active spreading and regional extension at Mount Etna imaged by SAR interferometry. Earth Planet Sci Lett 187:245–258

Gambino S, Mostaccio A, Patanè D, Scarfì L, Ursino A (2004) High-precision locations of the microseismicity preceding the 2002–2003 Mt. Etna eruption. Geophys Res Lett 31:L18604. DOI 10.1029/2004GL020499

Lo Giudice E, Rasà R (1992) Very shallow earthquakes and brittle deformation in active volcanic areas: the Etnean region as an example. Tectonophys 202:257–268

Lundgren P, Berardino P, Coltelli M, Fornaro G, Lanari R, Puglisi G, Sansosti E, Tesauro M (2003) Coupled magma chamber inflation and sector collapse slip observed with SAR interferometry on Mt. Etna volcano. J Geophys Res 108:2247–2261

Massonet D, Feigl KL (1998) Radar interferometry and its application to changes in the Earth's surface. Rev Geophys 36 (4):441–500

Nunnari G, Puglisi G (1997) Elaborazione dei dati geodimetrici sull'Etna; risultati preliminari. Boll GNV 1987:505–520

Obrizzo F, Pingue F, Troise C, De Natale G (2001) Coseismic displacements and creeping along the Pernicana Fault (Etna, Italy) in the last 17 years: a detailed study of a tectonic structure on a volcano. J Volcanol Geotherm Res 109:109–131

Obrizzo F, Pingue F, Troise G, De Natale G (2004) Bayesian inversion of 1994–1998 vertical displacements at Mt. Etna: evidence for magma intrusion. Geophys J Int 157:935–946

Okada Y (1985) Surface deformation due to shear and tensile fault in half-space. Bull Seismol Soc Am 75:1135–1154

Palano M (2003) InSAR techniques in structural geology: some applications to Mt. Etna volcano. PhD Thesis, Università degli Studi di Catania, Catania, Italy

Puglisi G, Bonforte A (2004) Ground deformation studies on Mt. Etna from 1995 to 1998 using static and kinematic GPS measurements. J Geophys Res 109:B11040. DOI 10.1029.2003JB002878

Puglisi G, Bonaccorso M, Bonforte A, Campisi O, Consoli O, Maugeri SR, Nunnari G, Puglisi B, Rossi M, Velardita R (1998) 1993–1995 GPS measurements on Mt. Etna: improvements in network configuration and surveying techniques. Acta Vulcanol 10:158–169

Puglisi G, Bonforte A, Maugeri SR (2001) Ground deformation patterns on Mt. Etna, between 1992 and 1994, inferred from GPS data. Bull Volcanol 62:371–384

Puglisi G, Briole P, Bonforte A (2004) Twelve years of ground deformation studies on Mt. Etna volcano based on GPS survey. In: Bonaccorso A, Calvari S, Coltelli M, Del Negro C, Falsaperla S (eds) Mt. Etna: volcano laboratory. Am Geophys Union Monogr 143:321–341

Reasenberg PA, Oppenheimer D (1985) FPFIT, FPPLOT AND FPPAGE: Fortran computer programs for calculating and displaying earthquake fault plane solutions. US Geol Surv Open-File Rep 85(739):1–109

Tibaldi A, Groppelli G (2002) Volcano-tectonic activity along structures of the unstable NE flank of Mt.Etna (Italy) and their possible origin. J Volcanol Geotherm Res 115:277–302